

Spatial correlations of mobility and immobility in a glassforming Lennard-Jones liquid

Claudio Donati¹, Sharon C. Glotzer¹, Peter H. Poole², Walter Kob³, and Steven J. Plimpton⁴

¹ *Polymers Division and Center for Theoretical and Computational Materials Science, NIST, Gaithersburg, Maryland, USA 20899*

² *Department of Applied Mathematics, University of Western Ontario, London, Ontario N6A 5B7, Canada*

³ *Institut für Physik, Johannes Gutenberg Universität, Staudinger Weg 7, D-55099 Mainz, Germany*

⁴ *Parallel Computational Sciences Department, Sandia National Laboratory, Albuquerque, NM 87185-1111*

(November 26, 2024)

Using extensive molecular dynamics simulations of an equilibrium, glass-forming Lennard-Jones mixture, we characterize in detail the local atomic motions. We show that spatial correlations exist among particles undergoing extremely large (“mobile”) or extremely small (“immobile”) displacements over a suitably chosen time interval. The immobile particles form the cores of relatively compact clusters, while the mobile particles move cooperatively and form quasi-one-dimensional, string-like clusters. The strength and length scale of the correlations between mobile particles are found to grow strongly with decreasing temperature, and the mean cluster size appears to diverge at the mode-coupling critical temperature. We show that these correlations in the particle displacements are related to equilibrium fluctuations in the local potential energy and local composition.

PACS numbers: 02.70.Ns, 61.20.Lc, 61.43.Fs

I. INTRODUCTION

The bulk dynamical properties of many cold, dense liquids differ dramatically from what might be expected from extrapolation of their high temperature behavior [1]. For example, many liquids cooled below their melting temperature exhibit rapid non-Arrhenius increases of viscosity and relaxation time with decreasing temperature, and two-step, stretched exponential decay of the intermediate scattering function $F(\mathbf{q}, t)$. Such behavior is often discussed as a “signature” of the approach to the glass transition. It has long been a central goal of theories of the glass transition to account for these bulk phenomena in terms of the microscopic dynamical motions of the molecules of the liquid. As a consequence, computer simulations of supercooled liquids, in which this microscopic information is immediately available, are increasingly used to complement theoretical and experimental efforts. In particular, simulations in recent years have focused on the study of “dynamical heterogeneity” to understand the microscopic origin of slow dynamics and stretched exponential relaxation in glass-forming liquids [2–6].

Recently we reported the observation of dynamical heterogeneity [7] and also cooperative molecular motion [8] in extensive molecular dynamics simulations of a supercooled Lennard-Jones (LJ) mixture. These spatially correlated dynamics were observed in a regime of temperature T , density ρ and pressure P for T above the dynamical critical temperature T_c obtained [9,10] from fits by the ideal mode coupling theory (MCT) [11] to other data on the same system. The principle goals of the present paper are twofold: (1) To test directly for spatial correlations of particles assigned (according to their displace-

ment over some time) to subsets of extreme mobility or immobility, and (2) to establish connections between this “dynamical heterogeneity” and local structure.

This paper is organized as follows. In Section II we present relevant background information, and in Section III we describe the model and computer simulation techniques. In Sec. IV, we examine the bulk dynamics and equilibrium structure of the liquid. In Sec. V we examine the mean square displacement and analyze the shape of the time-dependent distribution of particle displacements to define a time scale which we use to study dynamical heterogeneity throughout the remainder of the paper. In Sec. VI we group particles into subsets according to the maximum displacement they achieve on the time scale defined in the previous section, and show that particles of extremely high or low displacement are spatially correlated. From this we are able to identify a length scale that grows with decreasing T . In Sec. VII we show that fluctuations of the local mobility are correlated to fluctuations of the potential energy, or alternatively to fluctuations in the local composition of the liquid. In Sec. VIII we examine certain time dependent quantities associated with the observed dynamical heterogeneity, and finally in Sec. IX we conclude with a discussion.

II. BACKGROUND

It has been proposed that the stretched exponential behavior exhibited by the long time relaxation of $F(\mathbf{q}, t)$ can be attributed to a sum of many independent local exponential relaxations with different time constants, i.e., to a distribution of relaxation times [12]. This interpre-

tation is one form of the so-called “heterogenous” scenario for relaxation [6,12–17]. A number of recent experiments [13–15] have shown that in liquids such as orthoterphenyl and polystyrene within 10 K of their glass transition temperature T_g , subsets of molecules rotate slowly relative to the rest of the molecules on time scales long compared with collision times, but shorter than the relaxation time of density fluctuations. These liquids were thus termed “dynamically heterogenous.” None of these experiments were able to explicitly demonstrate whether slow molecules are spatially correlated, but typical distances over which slow molecules may be correlated were inferred [13].

There have been numerous attempts to indirectly measure a characteristic length scale over which molecular motions are correlated at the glass transition both in experiments [18–21] and in simulations [3,22]. Donth [18] relates the distribution of relaxation times in systems approaching their glass transition to equilibrium thermodynamic fluctuations having a characteristic size of ~ 3 nm at T_g . Thermodynamic measurements on orthoterphenyl [19], and dielectric measurements on salol [20], N-methyl- ϵ -caprolactan and propylene glycol [21], showed a shift in T_g due to confinement in pores of the order of a few nanometers. Mountain [3] showed that the size of regions that support shear stress in a simulation of a glass-forming mixture of soft spheres grows with decreasing temperatures. Monte Carlo simulations of polymer chains in two dimensions demonstrated strong finite size effects on diffusion [22]. A number of experiments and simulations on polymers confined to thin films all found a shift of T_g due to confinement [23–27]. These effects have all been attributed to the presence of cooperatively rearranging regions that grow with decreasing T . However, the origin of this characteristic length has never been shown explicitly. In particular, the connection of the characteristic length to a cooperative mechanism of molecular motion has not been experimentally demonstrated.

The intuitively-appealing picture of cooperative molecular motion was proposed in 1965 by Adam and Gibbs [28]. In their classic paper, they proposed that significant molecular motion in a cold, dense fluid can only occur if the molecules rearrange their positions in a concerted, cooperative manner. They postulated that a glass-forming liquid can be viewed as a collection of independently relaxing subvolumes within which the motion of the particles is cooperative. As the temperature of the liquid is lowered, the number of particles involved in cooperative rearrangements increases. If structural relaxation occurs through the cooperative rearrangement of groups of molecules, the liquid observed over a time-scale shorter than the structural relaxation time will appear as a collection of regions of varying mobility. These predictions can be tested by selecting subsets of molecules that relax slower (or faster) than the average, and determining

whether the molecules in a subset are randomly scattered through the sample or tend to cluster in a characteristic way.

The explicit connection between dynamical heterogeneity and cooperative motion is only recently being investigated experimentally in detail [20]. However, there have been a number of recent computational investigations addressing these issues. For example, Muranaka and Hiwatari [2] showed that displacements of particles measured over a timescale of the order of 5 collision times are correlated within a range of about two interparticle distances in a two-dimensional binary mixture of soft disks below the freezing point. Wahnström [29] showed that hopping processes in a strongly supercooled binary mixture are cooperative in nature. Hurley and Harrowell [4] identified fluctuating local mobilities in a supercooled two-dimensional (2-d) soft-disk system, and showed an example of correlated particle motion on a timescale of the order of 20 collision times. Mountain [3] demonstrated similar correlated particle motion in a 2-d supercooled Lennard-Jones mixture. By examining the time at which two neighboring particles move apart in 2-d and 3-d simulations of a supercooled soft-sphere mixture, Yamamoto and Onuki demonstrated the growth of correlated regions of activity [5]. They further studied the effect of shear on these regions [5], and showed that the size of the regions diminished in high shear. The clusters of “broken bonds” (denoting pairs of neighboring particles that separate beyond the nearest neighbor distance) identified in that work are similar in some respects to the clusters of highly mobile particles in a 3-d binary Lennard-Jones liquid reported previously by us [7], and described in detail in the present paper. The connection between the clusters of Ref. [7], which demonstrate a form of dynamical heterogeneity, and cooperative particle motion, was shown in Ref. [8].

III. SIMULATION DETAILS

We performed equilibrium molecular dynamics (MD) simulations of a binary mixture (80:20) of $N = 8000$ particles in three dimensions. The simulations were performed using the LAMMPS molecular dynamics code [30] which was designed for use on distributed memory parallel machines. LAMMPS partitions particles (atoms or molecules) across processors via a spatial decomposition [31] whereby each processor temporarily “owns” particles in a small fixed region of the simulation box. Each processor computes the motion of its particles and exchanges information with neighboring processors to compute forces and allow particles to migrate to new processors as needed.

The 6400 particles of type A and 1600 particles of type B interact via a 6-12 Lennard-Jones potential,

$$V_{\alpha\beta}(r) = 4\epsilon_{\alpha\beta} \left[\left(\frac{\sigma_{\alpha\beta}}{r} \right)^{12} - \left(\frac{\sigma_{\alpha\beta}}{r} \right)^6 \right], \quad (1)$$

where $\alpha\beta \in \{A, B\}$. The interaction forces between particles are zero for all $r > r_c = 2.5\sigma_{AA}$. Both types of particles are taken to have the same mass m . The Lennard-Jones interaction parameters $\epsilon_{\alpha,\beta}$ and $\sigma_{\alpha,\beta}$ for this mixture are: $\epsilon_{AA} = 1.0$, $\epsilon_{AB} = 1.5$, $\epsilon_{BB} = 0.5$, $\sigma_{AA} = 1.0$, $\sigma_{AB} = 0.8$, $\sigma_{BB} = 0.88$. Both the relative concentration of particle types and the interaction parameters were chosen to prevent demixing and crystallization [9]. Throughout this paper, lengths are defined in units of σ_{AA} , temperature T in units of ϵ_{AA}/k_B , and time t in units of $\sqrt{\sigma_{AA}^2 m / \epsilon_{AA}}$.

The simulations for each state point (P, T, ρ) are performed in three stages. First, a constant NPT adjustment run is performed by coupling the system to stochastic heat and pressure baths to bring the system from a nearby state point (usually the previously simulated state point) to the desired state point [32]. Second, a constant NVT equilibration run is performed to test for unwanted drifts in pressure P or potential energy U [33]. If no drift is observed, the final state of the system is considered to represent an equilibrium state of the system. Third, a constant NVE data-gathering run is performed using the final equilibrated state obtained from the second stage, and snapshots containing the particle coordinates and velocities are taken at logarithmic time intervals during the run. In this stage, the equations of motion are integrated using the velocity Verlet algorithm with a step size of 0.0015 at the highest temperature, and 0.003 at all other temperatures. All quantities presented here are calculated in this third stage. The analysis is performed by post-processing the snapshot files, which number as many as several thousand for the lower temperatures.

We simulated nine state points along a path in P, T, ρ that is linear when projected in the (P, T) plane. This path was chosen so that we would approach, from high temperature, the mode-coupling critical point $T_c = 0.435$, $P_c = 3.03$, $\rho_c = 1.2$ [9] along a path different from that used in Ref. [9]. Table 1 shows the values of P, T , and ρ for each state point.

For state points far above T_c (e.g. runs 1–5), the data-gathering runs required more cpu time than the equilibration. For state points nearer T_c , the equilibration stage was the most time consuming. In these cases the NVT stage of the simulations showed a slight drift of the pressure over time. To shorten the time required for complete equilibration, we estimated a new volume or temperature to create a nearby state point that we expected would be very nearly equilibrated with the current particle configuration. Then we instantaneously scaled the positions or velocities of the system (ie. adjusted the volume or temperature) and began another constant NVT run to test for equilibration. By iterating this procedure a few times we were able to find an equilibrated state point within

0.03% of the desired P and T at low temperatures.

At the lowest T studied ($T = 0.4510$), the total run time following equilibration is 1.2×10^4 time units. Thus, assuming Argon values for the parameters in Eq. 3.1, the data presented here extend up to 25.8 ns.

IV. STRUCTURE AND BULK RELAXATION

In this section, we show that the simulated liquid exhibits the characteristic features of an atomic glass-forming liquid.

Structural relaxation may be probed experimentally by the intermediate scattering function $F(\mathbf{q}, t)$, which is both the spatial Fourier transform of the van Hove correlation function $G(\mathbf{r}, t)$ and the inverse time transform of the dynamic structure factor $S(\mathbf{q}, \omega)$ [34]. In a computer simulation, the self (incoherent) part of the intermediate scattering function $F_s(\mathbf{q}, t)$ may be calculated directly from

$$F_s(\mathbf{q}, t) = \frac{1}{N_\alpha} \left\langle \sum_{j \in \alpha} e^{i\mathbf{q} \cdot (\mathbf{r}_j(t) - \mathbf{r}_j(0))} \right\rangle, \quad (2)$$

where $r_j(t)$ is the position of particle j at time t , and $\langle \dots \rangle$ indicates an average over independent configurations. This quantity describes the relaxation of density fluctuations due to single particle displacements on an inverse length scale $2\pi/q$, where $q \equiv |\mathbf{q}|$. If we assume rotational invariance of the system, $F_s(q, t)$ depends only on q . The time dependence of $F_s(q, t)$ for the A particles for $q = q_{max}$ is shown in Fig. 1. (Throughout this paper, q is chosen as q_{max} , the position of the first maximum of the static structure factor $S(q, 0)$). At high T , $F_s(q, t)$ decays to zero exponentially. As the system is cooled, $F_s(q, t)$ develops a plateau that separates a short time relaxation process from a long time relaxation process. This plateau indicates a transient “localization” of particles in the “cages” formed by their neighbors, and is a characteristic feature of all glassforming liquids.

The mode-coupling theory developed for supercooled liquids by Götze and Sjögren makes a number of predictions concerning the decay of the intermediate scattering function [11]. These predictions have been tested and verified for the LJ potential used here in a regime of P, T , and ρ similar but not identical to that simulated here [9]. There it was shown, e.g., that the early and late β -relaxation regimes are well described by power laws, and that the late time behavior of $F_s(q, t)$ exhibits time-temperature superposition with a time constant τ_α that diverges as a power law as T approaches $T_c \simeq 0.432$, with exponent $\gamma \simeq 2.7$. The diffusion constant was found to scale as $D \sim (T - T_c)^{-\gamma}$, with $\gamma = 2.0$ for the A particles, $\gamma = 1.7$ for the B particles, and $T_c = 0.435$.

The simulations performed in the present work extend from a point in the phase diagram where two-step relaxation begins to emerge, down to a state point that

is within approximately 4% of T_c . Over this range, we find that τ_α increases by 2.4 orders of magnitude, and fits well to the power law form found in Ref. [9], with approximately the same critical temperature and critical exponent.

It is well known that although relaxation becomes strongly nonexponential and relaxation times increase by many orders of magnitude as a supercooled liquid approaches a glass transition, changes in the static structure of most liquids are far less remarkable. To demonstrate this for our system, we examine the pair correlation functions $g_{\alpha\beta}(r)$ given by

$$g_{\alpha\beta}(\mathbf{r}) = \frac{V}{N_\alpha N_\beta} \left\langle \sum_{\substack{i \in \alpha \\ j \in \beta}} \delta(\mathbf{r} + \mathbf{r}_j - \mathbf{r}_i) \right\rangle, \quad (3)$$

for $\alpha \neq \beta$ and

$$g_{\alpha\alpha}(\mathbf{r}) = \frac{V}{N_\alpha(N_\alpha - 1)} \left\langle \sum_{i,j \in \alpha} \delta(\mathbf{r} + \mathbf{r}_j - \mathbf{r}_i) \right\rangle, \quad (4)$$

where N_α (N_β) is the total number of particles of species α (β). With this normalization, $g_{\alpha\beta}(\mathbf{r})$ converges to unity for $r \rightarrow \infty$ in the absence of long range correlations. Assuming rotational invariance, the correlation functions do not depend on the direction of the vector \mathbf{r} , but only on the distance $r = |\mathbf{r}|$.

In Figs. 2,3 and 4 we show the pair correlation functions $g_{AA}(r)$, $g_{AB}(r)$, and $g_{BB}(r)$ for three temperatures. The figures show that these functions do not change dramatically as a function of the state point. As the temperature is lowered, the main effect on all three functions is that the maxima and the minima become slightly more pronounced. Additionally, the second maximum of $g_{AA}(r)$ and $g_{AB}(r)$ at low T shows a splitting that has commonly been interpreted as a signature of an amorphous solid, although at these state points our system is an equilibrium liquid. Recently, evidence has been reported [35] that in a 2-d system of hard-disks the splitting of the second peak in the pair correlation function is due to the formation of regions with hexagonal close-packed order.

V. SINGLE PARTICLE DYNAMICS

Having established that the model liquid studied here exhibits the characteristic bulk phenomena of a glass-forming liquid, we examine in this section the distribution of individual particle motions.

The most basic dynamical bulk quantity that is easily accessible to simulation is the particle mean square displacement (MSD), $\langle r^2(t) \rangle$. Because we are investigating a binary mixture, we refer in the following to a MSD for the A particles and a MSD for the B particles. At high T , the MSD for both species exhibits two distinct regimes

(see Fig. 5). In the short time limit (regime I) the MSD is ballistic, i.e. $\langle r^2(t) \rangle \propto t^2$. For longer times (regime III), the MSD is diffusive, i.e. $\langle r^2(t) \rangle \propto t$. As the system is cooled, an intermediate regime (II) between these two limiting behaviors develops. Before entering the diffusive regime, $\langle r^2(t) \rangle$ exhibits a plateau, analogous to the plateau in the intermediate scattering function, that likewise arises from a transient ‘‘caging’’ of each particle by its neighbors. As seen in the figure, the time the system spends in the plateau depends strongly on T , and increases with decreasing T . The MSD for the B particles (not shown) exhibits qualitatively the same time dependence as shown in Fig. 5, but the diffusive regime is reached at shorter times, and the diffusion constant is larger, than for the A particles [9]. This difference can be explained by the different sizes of the A and B particles and by the fact that the interaction constant ϵ_{BB} is smaller than ϵ_{AA} .

In this paper, we are interested in whether spatial correlations exist between particles that exhibit either extremely large or extremely small displacements over some time interval. To determine this, we must first define the time interval over which the particle displacements will be monitored. Obviously, displacements may be monitored over any time interval, from the ballistic regime to the diffusive regime. To see whether there is a natural time scale on which the particle displacements might exhibit a particularly strong correlation, we turn to the self part of the van Hove correlation function, $G_s(r, t)$, which gives the probability to find a particle at time t at a distance r from its position at $t = 0$ [34]:

$$G_s(\mathbf{r}, t) = \frac{1}{N_\alpha} \left\langle \sum_i \delta(\mathbf{r} + \mathbf{r}_i(0) - \mathbf{r}_i(t)) \right\rangle. \quad (5)$$

Due to the rotational symmetry of the system, $G_s(\mathbf{r}, t)$ is a function of the modulus r of the vector displacement \mathbf{r} . The quantity $4\pi r^2 G_s(r, t)$, which gives the number of particles located a distance r from their original position at time t , is shown in Fig. 6 for the A particles for three different times at the lowest T . Also shown in Fig. 6 is the Gaussian approximation $4\pi r^2 G^0(r, t)$, where [34]

$$G^0(r, t) = \left(\frac{3}{2\pi \langle r^2(t) \rangle} \right)^{\frac{3}{2}} \exp \left(-\frac{3r^2}{2 \langle r^2(t) \rangle} \right) \quad (6)$$

and where $\langle r^2(t) \rangle$ is equal to the measured one. The Gaussian form appears to be a good approximation to $G_s(r, t)$ at both short and long times. However, it is apparent from the figure that $G_s(r, t)$ is significantly different from $G^0(r, t)$ at intermediate times. In particular, while many of the particles have traveled less than would be expected from the knowledge of $\langle r^2(t) \rangle$ alone, a small number of particles have traveled significantly farther. As a result, at intermediate times $G_s(r, t)$ displays a long tail that extends beyond one interparticle distance at $T = 0.4510$ (cf. Fig. 7).

This “long tail” behavior is most pronounced at a time t^* when $G_s(r, t)$ deviates most from a Gaussian (cf. Fig. 7) as characterized by the “non-Gaussian” parameter [36],

$$\alpha_2(t) = \frac{3\langle r^4(t) \rangle}{5\langle r^2(t) \rangle^2} - 1, \quad d = 3. \quad (7)$$

While one can define many different non-Gaussian parameters, this particular one involves the lowest possible moments. With this definition, $\alpha_2(t)$ is zero if $G_s(r, t)$ is Gaussian. If a distribution has a tail that extends to distances exceeding those for a Gaussian distribution with the same second moment, all higher order moments of this distribution will exceed those of the corresponding Gaussian, and consequently $\alpha_2(t)$ will assume positive values. In Fig. 8 we show $\alpha_2(t)$ for various T for the A particles. As expected, $\alpha_2(t)$ is zero at short times, then becomes positive, exhibits a maximum, and finally goes to zero at long times. As T decreases, the position of the maximum t^* shifts towards longer times, and the height of the maximum α_2^* increases. For all T , we find that t^* corresponds to times in the late- β /early- α relaxation regime. Furthermore, by dividing $\alpha_2(t)$ by α_2^* , and dividing t by t^* , one can show [37] that all curves collapse onto a single master curve for all times larger than the microscopic time (where they already collapse before scaling) [4,10,38]. This data collapse, which is likely related to the time-temperature superposition exhibited by the intermediate scattering function (but not trivially related, since t^* does not scale linearly with τ_α), suggests that t^* is in some sense a characteristic time for this system [37]. Note that t^* is orders of magnitude larger than the microscopic “collision time” [39] τ ; for example, at $T = 0.4510$ $t^* = 155.5$ and $\tau = 0.09$.

We see from an analysis of the temperature-dependent distribution of particle displacements at various times, and the calculation of the time-dependence of the non-Gaussian parameter, that the single particle dynamics is most non-Gaussian — and displays the widest range of possible behaviors — on the timescale t^* . The interval from zero to t^* thus provides a convenient choice over which to monitor the particle displacements and study their correlations because (i) since t^* is the time at which the distribution of particle displacements is broadest, it may also be when the liquid is likely to be most “dynamically heterogeneous”; and (ii) t^* is well-defined and easily calculated. Thus, throughout this paper we will use the time window from zero to t^* as the time interval over which the particle displacements are calculated, and over which we investigate dynamical heterogeneity.

VI. ANALYSIS OF SPATIAL CORRELATIONS OF PARTICLE DISPLACEMENTS

In this paper, we are interested in studying the extreme behavior of the individual particle motion, from the extremely mobile to the extremely immobile. In Refs. [7] and [8], we defined the magnitude of the displacement $u_i(t, t^*) \equiv |\mathbf{r}_i(t^* + t) - \mathbf{r}_i(t)|$ of particle i in a time interval t^* , starting from its position at an arbitrarily chosen time origin t , as a measure of the mobility of the i -th particle. At t^* , the distribution of u_i values is given by the self part of the van Hove correlation function, $G_s(r, t^*)$, where $r \equiv u$ (cf. Fig. 7). In Refs. [7,8] a subset of “mobile” particles was defined by selecting all the particles that in the interval $[0, t^*]$ had traveled beyond the distance r^* where $G_s(r, t^*)$ exceeds $G^0(r, t^*)$. With this definition, “mobile” particles are those that contribute to the long tail of the van Hove distribution function at the time t^* (cf. Fig. 7). In Refs. [7,8], it was shown that mobile particles selected according to this rule tend to cluster [7], and move cooperatively [8]. This definition of mobility given by the magnitude of particle displacement is thus sufficient to establish the phenomena of both dynamical heterogeneity and cooperative motion.

Intuitively, we think of immobile particles as those particles which are trapped in cages formed by their neighbors. Nevertheless, particles do not sit at one position; they essentially “oscillate” back and forth within the cage formed by their neighbors. To study correlations between the most immobile particles, we need a definition of mobility which allows us to select the particles for which the amplitude of this oscillation (ie. the maximum displacement of the particle) is the smallest. In this paper, we therefore define the mobility $\mu_i(t)$ of the i -th A particle as the *maximum* distance reached by that particle in the time interval $[t, t + t^*]$:

$$\mu_i(t) = \max_{t' \in [0, t^*]} \{ |\mathbf{r}_i(t' + t) - \mathbf{r}_i(t)| \} \quad (8)$$

This new definition of mobility, which we use throughout this paper, allows us to examine different subsets of particles, from the most to the least mobile, in the same way. As a compromise between examining the most extreme behavior and including enough particles to obtain good statistics when examining their spatial correlation (i.e. maximizing the signal-to-noise ratio), we will examine the 5% most mobile and 5% least mobile particles. *Thus we define as “mobile” the 5% of all particles having the highest values of $\mu(t)$, and “immobile” the 5% having the lowest value.* Note that this new definition of mobility does not qualitatively change the results obtained previously in [7,8], provided that the new definition selects approximately the same fraction of the sample as the definition previously used (approximately 5.5% in Ref. [7]) Compare, for instance, Figs. 11 and 12 with Fig. 3 of Ref. [7].

The subsets of mobile particles selected using the definition of Ref. [7] and that used here have a large overlap, since particles that have moved relatively far at some time in the interval $[0, t^*]$ are likely to remain relatively far at the end of the interval. However, subsets of immobile particles selected with the two different rules do not have as large an overlap, since a particle with a small displacement at some time may have previously traveled far, and then returned to its original position. The distribution $4\pi\mu^2 P(\mu, t^*)$ at t^* is shown in Fig. 9. For comparison, the probability distribution $4\pi r^2 G_s(r, t^*)$ is also shown. Note that, although at t^* particles can be found arbitrarily close to their position at $t = 0$, $P(\mu, t^*)$ is zero for $\mu < 0.17$.

In Fig. 10, we show the 320 mobile particles (light spheres) and the 320 immobile particles (dark spheres) at the beginning of an arbitrary time interval $[t, t + t^*]$ for one configuration at $T = 0.4510$. The other 7360 particles are not shown. The figure shows that particles of similar mobility are spatially correlated and that particles with different mobility tend to be anticorrelated. These correlations can be quantitatively studied by calculating static pair correlation functions between particles belonging to the different subsets.

In Fig. 11 we show the pair correlation function $g_{MM}(r)$ between mobile particles for four different temperatures. $g_{MM}(r)$ is defined by Eq. 4 with the sum restricted to the mobile particles. For all T , $g_{MM}(r)$ is appreciably higher than the average $g_{AA}(r)$ (cf. Fig. 2) for all r . The “excess” correlation given by the ratio $\Gamma(r) = [g_{MM}(r)/g_{AA}(r)] - 1$ is plotted as a function of r in Fig. 12. With the exception of the excluded volume sphere of the LJ potential, $\Gamma(r) > 0$ at intermediate distances and converges to zero for large r . It is clear from the figure that the total excess correlation, given by the area under the curve, increases with decreasing T .

We can obtain an estimate of the typical distance over which mobile particles are correlated by identifying clusters of nearest-neighbor mobile particles [40]. To do this, we use the following rule: two particles belong to the same cluster if their distance at $t = 0$ is less than r_{nn} , the radius of the nearest neighbor shell, which is defined by the first minimum in $g_{AA}(r)$ and has a weak temperature dependence. In our hottest run $r_{nn} = 1.45$, while in the coldest run $r_{nn} = 1.40$. The distribution $P(n)$ of clusters of size n is shown in Fig. 13. Although most of the clusters have only a modest size, the data show that a significant fraction of the mobile particles, which themselves make up only 5% of the sample (320 particles), are part of big clusters. For instance, at $T = 0.4510$, there is typically at least one cluster in each configuration that contains ≈ 100 particles. For that T , $P(n) \sim n^{-\tau}$ with $\tau = 1.86$. In the inset we show the mean cluster size $S = \sum n^2 P(n) / \sum n P(n)$ [41], plotted log-log versus $T - T_c$, where $T_c = 0.435$ is the fitted critical temperature of the mode coupling theory [9,10]. Although there is less

than a decade on either axis, the figure shows that the temperature dependence of S is consistent with a divergence at T_c of the form $S \sim (T - T_c)^{-\gamma}$, with $\gamma \approx 0.618$. Note that MCT makes no predictions about clustering or the divergence of any length scales as the critical point is approached [42].

To test the sensitivity of the apparent percolation transition at the mode-coupling temperature, we repeat the cluster size distribution analysis for the 3% and 7% most mobile particles. For each subset, the mean cluster size S is shown vs. $T - T_c$ in Fig. 14. The best fit of $S \sim (T - T_p)^{-\gamma}$ to each set of data gives $T_p = 0.440$ for the set containing the 3% most mobile particles, $T_p = 0.431$ for the set containing the 5% most mobile particles, and $T_p = 0.428$ for the set containing the 7% most mobile particles. However, within the accuracy of the data the three sets are also consistent with a divergence at T_c . If we further increase the fraction of mobile particles beyond the fraction corresponding to a random close-packed percolation transition [43], the mobile particles percolate and most of the mobile particles are found in a single cluster that spans the whole simulation box.

In Fig. 15 we show one of the largest clusters of mobile particles found in our coldest simulation. It is evident from the figure that these clusters cannot be described as compact, as often supposed either implicitly or explicitly in phenomenological models of dynamically heterogeneous liquids [13,44]. Instead, the clusters formed by the mobile particles appear to have a disperse, string-like nature. As discussed in [8], a preliminary calculation of the fractal dimension of the clusters, although hampered by a lack of statistics, indicates that the clusters have a fractal dimension close to 1.75, similar to that for both self-avoiding random walks and the backbone of a random percolation cluster in three dimensions [45].

In Ref. [8], it was shown that this quasi-one-dimensionality appears to arise from the tendency for mobile particles to follow one another. This is demonstrated in Fig. 16, where we plot the time-dependent pair correlation function for the mobile particles, $g_{MM}(r, t^*)$ for different temperatures. At $t = 0$, this function coincides with $g_{MM}(r)$ in Fig. 11. For $t > 0$, the nearest neighbor peak moves toward $r = 0$, demonstrating that a mobile particle that at $t = 0$ is a nearest neighbor of another mobile particle tends to move toward that particle at later times. We find that the peak at $r = 0$ is highest near $t = t^*$, and decreases for later times. A small but discernable peak at $r = 0$ is also present in $g(r, t^*)$ [46].

Fig. 17 shows a cluster of mobile particles at two different times, $t = 0$ and $t = t^*$, to demonstrate the cooperative, string-like nature of the particle motion.

In a manner identical to our analysis of the mobile particles, we define as immobile the 5% of the A particles that have the lowest value of μ . The pair correlation function $g_{II}(r)$ between immobile particles shown in Fig. 18 shows that these particles also tend to be spatially corre-

lated. It is interesting to note that while the maxima in $g_{II}(r)$ are higher at all T than the corresponding maxima in $g_{AA}(r)$, the depth of the minima does not change appreciably for the lowest temperatures. Fig. 19 shows the ratio $\Gamma(r) = [g_{II}(r)/g_{AA}(r)] - 1$ as a function of r . In contrast to what we find for the most mobile particles, the correlation between immobile particles does not show any evidence of singular behavior as T decreases. Instead, the correlation appears to grow and then “saturate” to some limiting behavior for all $T < 0.468$. Moreover, Fig. 19 shows that the local structure of the liquid appears to be more ordered in the vicinity of an *immobile* A particle than in the vicinity of a *mobile* A particle.

In Fig. 20 we show the size distribution of the clusters of immobile particles, formed with the same rule used for the mobile ones. One of the largest clusters found at $T = 0.4510$ is shown in Fig. 21. In the inset of Fig. 20 we show the mean cluster size S versus $T - T_c$. We find that the mean cluster size of immobile particles is relatively constant with T . This may be because immobile particles are relatively well-packed, and cannot grow beyond some limiting size [47]. Or, these clusters may be the “cores” of larger clusters of particles with small displacements, that may grow with decreasing T . To elucidate this, more particles (e.g. the next 5% higher mobility) should be included in the analysis. We will return to this important point and provide further relevant data in the next section.

The correlation between mobile and immobile particles, measured by the pair correlation function $g_{MI}(r)$ (Fig. 22), shows that mobile and immobile particles are anti-correlated. A comparison between $g_{MI}(r)$ and $g_{AA}(r)$, shown in Fig. 23, demonstrates that, over several interparticle distances, the probability to find an immobile A particle in the vicinity of a mobile one is lower than the probability to find a generic A particle. The figure also shows that the characteristic length scale of the anticorrelation grows with decreasing T . This length scale does not show a tendency to diverge as T_c is approached. In particular, the curves for the two coldest runs (and closest to T_c) are almost coincident.

VII. LOCAL ENERGY AND LOCAL COMPOSITION VS. MOBILITY

We have seen in the previous section that despite the lack of a growing static correlation, a growing *dynamical* correlation — characterizing spatial correlations between particles of similar mobility — does exist. These correlations must therefore arise from subtle changes in the local environment that are not completely captured by the usual static pair correlation function. In this Section, we calculate several quantities to elucidate whether the mobility of a particle is related to its potential energy, and to the composition of its local neighborhood.

In Fig. 24 we show the distributions of the potential energies of the 5% most mobile, 5% least mobile, and all particles at $T = 0.4510$, calculated at the beginning of an arbitrary time interval $[t, t + t^*]$. The distributions have been normalized such that the area under each curve is one. The distributions differ by a small relative shift of the mean value, approximately 3% for the high mobility distributions and somewhat less for the low mobility distribution. We find that the magnitude of the shift increases with decreasing T , but the *relative* shift appears to be *independent* of T . Since the liquid is in equilibrium, this shift will vanish for $t \rightarrow \infty$. Thus, not suprisingly, mobile particles are those that in a time t^* are able to rearrange their position so as to lower their potential energy. It is worth noting that the mobility does not show any correlation with the kinetic energy of the particles measured at $t = 0$. The kinetic energy distributions of the subsets with different mobility coincide exactly with the average distribution, showing that the mobility cannot be related to the presence of “hot spots” in the liquid.

We next divide the entire population of A particles into 20 subsets, each composed of 5% of the particles. In the first subset we put the 5% of the particles with the highest values of μ (the mobile particles defined above), in the second subset the next 5%, and so on. The last subset thus contains the 5% most immobile particles. In Fig. 25 we plot (on the x-axis) the average mobility of each subset versus (on the y-axis) the average potential energy of that subset at $t = 0$. We find that the subset with the lowest mobility is also the one with the lowest potential energy. We also find that as the potential energy increases, the mobility increases. We see from the figure that the mobile particles are the subset with the highest average potential energy at $t = 0$.

Two more points are worth noting in Fig. 25. First, at all T the mobile particles move, on average, approximately one interparticle distance in the time interval $[0, t^*]$. Second, for all T the difference in both mobility and potential energy between the 5% most mobile particles and the next subset is significantly larger than between any other two consecutive subsets. This observation suggests that the choice of 5%, while arbitrary, is a reasonable one. As shown in the figure, the separation between the 5% most mobile particles and the next subset shows a tendency to grow with decreasing T . Note however, that the distance between the lowest mobility subset and the next subset *decreases* with decreasing T , making it very difficult in the current approach to define an appropriate subset containing particles whose mobility is distinctly lower than the rest. This, together with the result that the mean cluster size of immobile particles is relatively constant over the range of temperatures studied, suggests that our analysis of the lowest subset is inadequate to fully characterize clusters of particles which do not move a substantial distance [48].

Thus we see that the gross structural information con-

tained in the potential energy is sufficient to establish a general correlation between energy and mobility. However, as seen in Fig. 24, the distribution of potential energies of mobile particles overlaps for most of the range of the abscissa with the distribution for the generic A particles. *Thus, it is not possible to decide if a certain particle is mobile on the basis of that particle's instantaneous potential energy alone.* Other factors, such as defects in the local packing, and the relative potential energy of neighboring particles, must contribute as well.

The relation between mobility and potential energy suggests a relation between mobility and local composition. Indeed, a calculation of the pair correlation functions $g_{MA}(r)$ and $g_{MB}(r)$ (see Figs. 26 - 29) between a mobile particle and a generic A or B particle, respectively, shows that, on average, a mobile A particle tends to have less B particles, and more A particles, in its nearest neighbor shell than a generic A particle.

A correlation can also be found between *immobility* and small composition fluctuations of the mixture. A comparison of $g_{AB}(r)$ to the pair correlation function $g_{IB}(r)$, which measures the number of B particles a distance r from a test immobile A particle, shows that an immobile A particle has, on average, more B particles in its nearest neighbor shell than does a generic A particle. As shown in Fig. 30, where the ratio $[g_{IB}/g_{AB}(r)] - 1$ is plotted as a function of r , this enhanced correlation is independent of T , and therefore does not suggest any evidence of $A - B$ phase separation (recall that the chosen energy parameters preclude $A - B$ phase separation).

From these results it is clear how a correlation between mobility and local composition causes a correlation between mobility and potential energy. Since the attractive interaction between A and B particles is stronger than either the attractive AA or BB interaction, the presence of a B between two A's reduces their potential energy. A particles in a B-rich region can thus be expected to have a reduced mobility. A particles in a B-poor region, however, will have a higher potential energy, resulting in a higher mobility.

VIII. STRUCTURAL RELAXATION OF PARTICLE SUBSETS AND DYNAMICAL HETEROGENEITY

We have shown that it is possible to select subsets of particles according to their maximum displacement over a timescale in the region of the late β -early α relaxation. We have also shown that the particles belonging to subsets selected at the extrema of the mobility spectrum are spatially correlated, and are related to small fluctuations in the local potential energy, and, consequently, in the local composition of the mixture. All of the data presented here suggest that this supercooled liquid contains fluctuations in local mobility, with diffuse, quasi-

one-dimensional regions of high mobility, and relatively compact regions of low mobility.

To measure how long a mobile particle will continue to be mobile, we define a variable $\nu_i^M(t)$ as 1 if the i -th particle belongs to the subset of the 5% most mobile particles in the interval $[t, t + t^*]$, and 0 otherwise. The function $\sigma_M(t)$

$$\sigma_M(t) = \frac{1}{n_M - \frac{n_M^2}{N_A}} \left(\sum_i \langle \nu_i^M(t) \nu_i^M(0) \rangle - \frac{n_M^2}{N_A} \right), \quad (9)$$

measures the fraction of particles that are mobile in the interval $[0, t^*]$ and still mobile in the interval $[t, t + t^*]$, when the time origin is shifted by t . Here n_M is the number of mobile particles (320 in the present case), and N_A is the total number of A particles (6400). The second term on the right-hand side of Eq. 9 is the number of particles that by random statistics would be classified as mobile in both time intervals. The normalization of $\sigma_M(t)$ is chosen so that $\sigma_M(0) = 1$. The results for $\sigma_M(t)$ for the coldest T are shown in Fig. 31.

We have also measured the fraction of particles that are immobile in the interval $[0, t^*]$ and still immobile in the interval $[t, t + t^*]$. Analogous to the case for the mobile particles, we define $\sigma_I(t)$ as

$$\sigma_I(t) = \frac{1}{n_I - \frac{n_I^2}{N_A}} \left(\sum_i \langle \nu_i^I(t) \nu_i^I(0) \rangle - \frac{n_I^2}{N_A} \right), \quad (10)$$

where n_I is the number of immobile particles (320) and $\nu_i^I(t)$ is a function that is 1 if the i -th particle is an immobile one in the interval $[t, t + t^*]$, and 0 otherwise. The function $\sigma_I(t)$ is also shown in Fig. 31.

The functions $\sigma_M(t)$ and $\sigma_I(t)$ are memory functions of mobility. When they have decayed to zero, there are no particles that have retained memory of their mobility in the initial time interval. Because a particle's mobility is based upon a criterion that depends on t^* , certain time-dependent functions measured for these subsets will have some "kink" at t^* . If a different t^* is chosen, the kink will move to the new t^* . In this respect, there is no "natural" lifetime for these clusters — by definition, they survive for a time t^* [50].

Nevertheless, we can obtain information from the form of the decay both before and after t^* . Because the data was stored not less than every 3 time units, we are unable to calculate $\sigma_M(t)$ and $\sigma_I(t)$ for $t < 3$. However, we see that these functions decay substantially before this time, since already at $t = 3$ both functions are significantly smaller than one. After this initial short-time relaxation, a second decay of both functions is observed up to $t = t^*$. At this time, a third decay process appears for the mobile particles, and possibly also for the immobile particles. The main point of Fig. 31 is that beyond t^* , both functions are less than 0.1. Thus there is only

a small tendency for particles to retain memory of their mobility beyond the initial time interval [51].

Thus, mobile and immobile regions do not persist beyond the time t^* over which the particle mobility is monitored. After the observation time, mobile and immobile particles maintain little memory of their previous state. Therefore the strong correlations found between particles must arise from the motion itself. If, for instance, the mobility of a particle and its spatial correlation with other particles of similar mobility could be explained solely by local fluctuations in quantities like density or composition, the mobility should persist until these fluctuations decay to zero. Instead, the dependence of the lifetime on the observation time can be explained if one assumes that particles can move only in a cooperative manner. Indeed, as was shown in Ref. [8], clusters of mobile particles like that shown in Fig. 15 can be decomposed into numerous, smaller string-like clusters (“strings”) of particles which follow one another in a cooperative fashion.

Fig. 32 shows the intermediate scattering functions $F_s^M(q, t)$ and $F_s^I(q, t)$, defined as the spatial Fourier transform of the self part of the van Hove correlation function $G_s^M(r, t)$ or $G_s^I(r, t)$ of the mobile and immobile particles, respectively. Both functions are identical to the bulk $F_s(q, t)$ for times less than the “collision time” $\tau = 0.09$ [39]. The figure shows that a two-step relaxation process occurs for the mobile particles, although the height of the plateau is smaller than for the bulk. The presence of the plateau in $F_s^M(q, t)$ indicates that the mobile particles are subject to the same “cage effect” experienced by the other particles, although the effective cage “size” and “lifetime” are different. Thus clusters of mobile particles should not be thought of as “fluidized” regions of the liquid in the simple sense that those regions might behave like high temperature or low density liquids. Instead, the difference between the mobile particles and the rest of the sample appears to be, from the point of view of the single particle dynamics, that they “escape” the cage earlier than the other particles.

We also see that the three curves in Fig. 32 cannot be superimposed by scaling the time axis in the same way as one can superimpose $F(q, t)$ curves for different temperatures. Again, this indicates that the mobile and immobile subsets are not simply “hotter” or “colder” subsets of the sample, in agreement with the perfect superposition of the kinetic energy distributions.

In contrast to the bulk average $F_s(q, t)$, $F_s^M(q, t)$ is not a monotonically decreasing function of time. For times longer than t^* , a small but clearly detectable increase of the function can be noticed in Fig. 32. This behavior can be interpreted as a tendency of a small fraction of the particles that we have selected to return towards their position at the beginning of the selection interval. These particles may also be those that contribute to the small memory effect observed in $\sigma_M(t)$ in Fig. 31, but further analysis is required to establish this connection.

Finally, we show in Fig. 33 the fraction ϕ of particles that at time t have not yet been labeled mobile. This function is calculated by labeling the mobile particles in the first interval $[0, t^*]$, and then shifting the interval by t and reassigning the particle mobilities. Thus at $t = 0$, 95% of the particles have not been labeled mobile. In the interval $[t, t + t^*]$, more particles will have been labeled mobile, so ϕ will decrease. We have normalized $\phi(t)$ such that $\phi(0) = 1$. Also shown in Fig. 33 is the long-time α -relaxation part of the bulk $F_s(q, t)$ for $q = q_{max}$. Fits to both functions are also shown. Both functions fit well to a stretched exponential $y(t) = A \exp[(-t/\tau)^\beta]$ with $\beta = 0.75$ and $\tau_\alpha = 655$ for the intermediate scattering function, and with $\beta = 0.78$ and $\tau_\alpha = 475$ for ϕ . That both functions have a similar form (similar β), and similar time constants, suggests that the process by which immobile particles become mobile governs the long time structural relaxation of density fluctuations at wavevectors corresponding to the peak of the static structure factor. Moreover, it demonstrates that the “arbitrary” choice of 5% represents a physically meaningful fraction of the system .

IX. DISCUSSION

In this paper, we have described an investigation of the individual particle dynamics of a cold, dense Lennard-Jones mixture well above the glass transition in an effort to discover if the liquid is dynamically heterogeneous, and if so to determine the extent and nature of the dynamical heterogeneity. Since there were no quantitative theoretical predictions regarding this matter, the approach we have taken is exploratory; particle trajectories were saved during the course of the simulation and then analyzed and visualized in numerous ways. We find that this supercooled liquid is “dynamically heterogeneous” because particles with similar mobility are spatially correlated. Note that our definition of heterogeneity is different from the one used, for instance, in 4-D NMR experiments, where the system is defined as heterogeneous if a slow subset remains slow for times longer than the average relaxation time [14]. We further find that highly ramified clusters of mobile particles grow with decreasing T and appear to percolate at the mode-coupling temperature. This is the first evidence for a percolation transition coincident with T_c , and it is very different from the type of percolation transition proposed in free volume theory [52]. It is especially interesting since MCT does not make any predictions regarding clusters or diverging length scales. We also find that particles of low mobility form relatively well-ordered, compact clusters which do not appear to grow with decreasing T if the number of immobile particles included in the subset is kept constant. Although mobile and immobile clusters are anti-correlated, there is no tendency towards bulk phase

separation of mobile and immobile regions because of the highly ramified, extended nature of the mobile regions.

In our analysis, we find no evidence to support a picture in which the system can be thought of as a collection of subvolumes that each relax independently and simultaneously with their own time constant. Instead, it appears that at any given time, most particles are localized in cages and a small percentage of particles form large clusters of smaller, cooperatively rearranging “strings.” After rearranging, these mobile particles become caged themselves, and others become mobile. This process repeats until, on the time scale of the α relaxation, each particle has rearranged at least once. Thus the structural relaxation of the liquid appears to be highly cooperative in the spirit of Adam and Gibbs, but where different subvolumes of the liquid are able to relax only after other subvolumes relax. This will be further explored in a separate publication [49].

PHP acknowledges the support of NSERC. WK is partially supported by Deutsche Forschungsgemeinschaft under SFB 262. CD and SCG thank Jack Douglas for many interesting discussions.

Corresponding author: sharon.glotzer@nist.gov.

-
- [1] For a summary of phenomenology and theory on glasses and supercooled liquids, see eg. recent issue of Science [297, 1945 (1995)] and M. D. Ediger, C. A. Angell, S. R. Nagel, J. Phys. Chem. **100**, 13200 (1996).
- [2] T. Muranaka and Y. Hiwatari, Phys.Rev.E **51**, R2735 (1995).
- [3] R.D. Mountain, J.Chem.Phys. **102**, 5408, (1995); R. D. Mountain, in “Supercooled Liquids: Advances and Applications”, Proc. Amer. Chem. Soc., New York (1997) pg. 122;
- [4] M. Hurley and P. Harrowell, Phys. Rev. E **52**, 1694 (1995).
- [5] R. Yamamoto and A. Onuki, Phys. Rev E, in press.
- [6] B. Doliwa and A. Heuer, Phys. Rev. Lett. **80**, 4915 (1998); A. Heuer, K. Okun, J. Chem. Phys. **106**, 6176 (1997).
- [7] W. Kob, C. Donati, S.J. Plimpton, P.H. Poole and S.C. Glotzer, Phys. Rev. Lett. **79**, 2827 (1997).
- [8] C.Donati, J.F.Douglas, W.Kob, S.J.Plimpton, P.H. Poole and S.C.Glotzer, Phys.Rev.Lett. **80**, 2338 (1998).
- [9] W. Kob and H.C. Andersen, Phys. Rev. Lett. **73** 1376, 1994; W. Kob and H. C. Andersen, Phys. Rev. E **52**, 4134 (1995).
- [10] W. Kob and H. C. Andersen, Phys. Rev. E **51**, 4626 (1995);
- [11] W. Götze and L. Sjögren, Rep. Prog. Phys. **55**, 241 (1992).
- [12] J. R. Richert, J. Non-Cryst. Solids, **172-174**, 209 (1994); J. Phys. Chem **101**, 6323 (1997).
- [13] F. R. Blackburn, M. T. Cicerone, G. Hietpas, P. A. Wagner, M. D. Ediger, J. Non-Cryst. Solids **172-174**, 256 (1994).
- [14] K. Schmidt-Rohr and H.W. Spiess, Phys. Rev. Lett. **66**, 3020 (1991); J. Leisen, K. Schmidt-Rohr and H. W. Spiess, J. Non-Cryst. Solids **172-174** 737 (1994); A. Heuer, M. Wilhelm, H. Zimmermann and H.W. Spiess, Phys. Rev. Lett. **95**, 2851 (1995)
- [15] M.T. Cicerone, F.R. Blackburn and M.D. Ediger, J. Chem. Phys. **102**, 471 (1995); M.T. Cicerone and M.D. Ediger, J. Chem. Phys. **103**, 5684 (1995); F. Fujara, B. Geil, H. Sillescu and G. Fleischer, Z. Physik B **88**, 195 (1992).
- [16] A. Heuer, Phys. Rev. E **56**, 730 (1997).
- [17] H. Sillescu, J. Non-Cryst. Solids (in press).
- [18] E. Donth, Physica Scripta **T49**, 223 (1993).
- [19] C.L. Jackson and G.B. McKenna. J.Non-Cryst. Solids **131-133** , 221 (1991).
- [20] M. Arndt, R. Stannarius, H. Grootheus, E. Hempel, F. Kremer, Phys. Rev. Lett. **79**, 2077 (1997); A. Huwe, M. Arndt, F. Kremer, C. Haggemüller and P. Behrens, J. Chem. Phys. **107** (1997); A. Schönals, R. Stauga, J. Chem. Phys. **108**, 5130 (1998).
- [21] G. Barut, P. Pissis, R. Pelster and G. Nimtz, Phys. Rev. Lett. **80**, 3543 (1998).
- [22] P. Ray and K. Binder, Europhys. Lett **27**, 53 (1994).
- [23] B. Jerome and J. Commandeur, Nature **386**, 589 (1997).
- [24] W. E. Wallace, J. H. Van Zanten and W. L. Wu, Phys. Rev. E **52**, R3329 (1995).
- [25] J. A. Forrest, K. Dalnoki-Veress and J. R. Dutcher, Phys. Rev. E **56**, 5705 (1997).
- [26] K. F. Mansfield and D. N. Theodoru, Macromolecules **23**, 4430 (1990); K. F. Mansfield and D. N. Theodoru, Macromolecules **24**, 6283 (1991).
- [27] J. Baschnagel and K. Binder, Macromolecules **28**, 6808 (1995); J. Baschnagel and K. Binder, J. Phys. I **6**, 1271 (1996).
- [28] G. Adam and J.H. Gibbs, J. Chem. Phys. **43**, 139 (1965).
- [29] G. Wahnström, Phys. Rev. A **44**, 3752 (1991).
- [30] S. J. Plimpton, R. Pollock, and M. Stevens, ”Particle-Mesh Ewald and rRESPA for Parallel Molecular Dynamics Simulations”, in Proc of the Eighth SIAM Conference on Parallel Processing for Scientific Computing, Minneapolis, MN, March 1997.
- [31] S. J. Plimpton, J. Comp. Phys. **117**, 1, (1995).
- [32] S. Melchionna, G. Ciccotti, and B. L. Holian, Molecular Physics, **78**, 533 (1993); W. G. Hoover, Phys. Rev. A **31**, 1695 (1985).
- [33] S. Nose, Molecular Physics **52**, 255 (1984).
- [34] J.P. Hansen and I.R. McDonald, “Theory of Simple Liquids”, Academic Press, London (1976).
- [35] T.M Truskett, S. Torquato, S. Sastry, P.G. Debenedetti and F.H. Stillinger, Phys. Rev. E, in press.
- [36] A. Rahman, Phys. Rev. A **136**, 405 (1964); K. Sköld, J. M. Rowe, G. Ostrowski and P. D. Randolph, Phys. Rev. A **6**, 1107 (1972).
- [37] C. Donati and S.C. Glotzer, in preparation.
- [38] F. Sciortino, P. Gallo, P. Tartaglia and S.-H. Chen, Phys. Rev. E **54**, 6331 (1996).
- [39] Here we have defined the “collision” time to be the time when the velocity autocorrelation function first changes

sign.

- [40] Statically defined clusters in liquids have been reported in a number of computational studies. See for example: Y. Hiwatari, *J. Chem. Phys.* **76**, 5502 (1982); R. M. J. Cotterill, *Phys. Rev. Lett.* **42**, 1541 (1979); S.-P. Chen, T. Egami and V. Vitek, *Phys. Rev. B* **37**, 2440 (1988); A. I. Mel'cuk, R. A. Ramos, H. Gould, W. Klein and Raymond D. Mountain, *Phys. Rev. Lett.* **75**, 1995); T. Tomida and T. Egami, *Phys. Rev. B* **52**, 3290 (1995); V. P. Voloshin, Y. I. Naberhukin, N. N. Medvedev and M. S. Jhon, *J. Chem. Phys.* **102** (1995); G. Johnson, A. I. Mel'cuk, H. Gould, W. Klein, R. D. Mountain, *Phys. Rev. E* **57** 5707 (1998); M. Li, preprint.
- [41] To take into account the possibility that the mobile particles percolate in our simulation box at $T > T_p$, we discard the largest cluster in each configuration in the calculation of S ; D. Stauffer and N. Jan, private communication.
- [42] However, there have been several computational studies which suggest some type of growing dynamical length scale as the glass transition is approached. See, e.g. Ref. [3,22].
- [43] Barry D. Hughes, *Random Walks and Random Environments* (Clarendon Press, Oxford, 1996).
- [44] F. H. Stillinger and J. A. Hodgdon, *Phys. Rev. E* **50**, 2064 (1994).
- [45] D. Stauffer, *Introduction to Percolation Theory* (Taylor and Francis, 1985).
- [46] J.L. Barrat, J.N. Roux, J.P. Hansen, *Chem. Phys.* **149**, 197 (1990); H. Miyagawa, Y. Hiwatari, B. Bernu, J.P.Hansen, *J. Chem. Phys.* **86**, 3879 (1988).
- [47] D. Kivelson and G. Tarjus, *Phil. Mag. B* **77**, 245 (1998), and references therein.
- [48] A more promising approach in this direction is to group particles according to their first passage time; see Ref. [49].
- [49] P. Allegrini, C. Donati, J.F. Douglas and S.C. Glotzer, in preparation.
- [50] However, there is a natural time at which the spatial correlation of particle mobilities is the most pronounced. See S.C. Glotzer, C. Donati and P.H. Poole, "Spatially-Correlated Dynamics in Glass-forming Systems: Correlation Functions and Simulations", in *Computer Simulations in Condensed Matter Physics XI*, ed. D.P. Landau, et al. Springer-Verlag, in press.
- [51] We have observed that a small fraction of mobile particles have a tendency to return to their initial positions at times longer than t^* . These particles may be responsible for this small memory effect, but further analysis needs to be done.
- [52] G.S. Grest and M.H. Cohen, *Adv. Chem. Phys.* **48**, 454 (1981).

Run	T	P	ρ
1	0.5495	0.4888	1.0859
2	0.5254	1.0334	1.1177
3	0.5052	1.4767	1.1397
4	0.4899	1.8148	1.1553
5	0.4795	2.0488	1.1651
6	0.4737	2.1746	1.1705
7	0.4685	2.2959	1.1757
8	0.4572	2.5490	1.1856
9	0.4510	2.6800	1.1910

Table 1: Temperature T , pressure P and density ρ of the nine state points simulated.

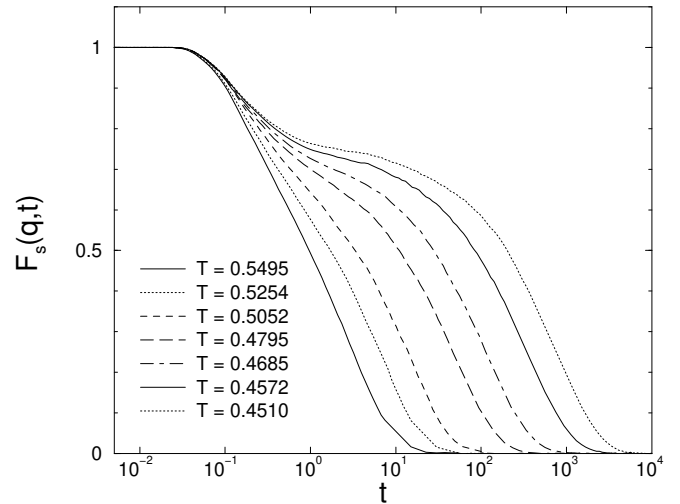


FIG. 1. Incoherent (self) intermediate scattering function $F_s(q, t)$ for $q_{max} = 7.12$.

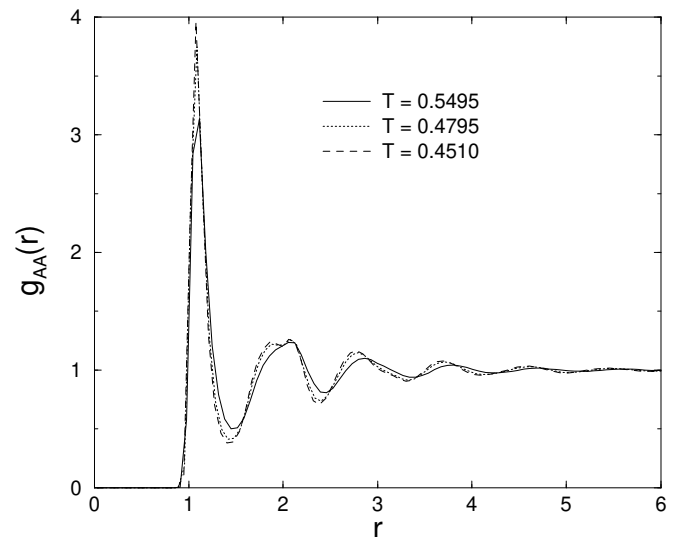


FIG. 2. Pair correlation function $g_{AA}(r)$ of the A particles for three different temperatures.

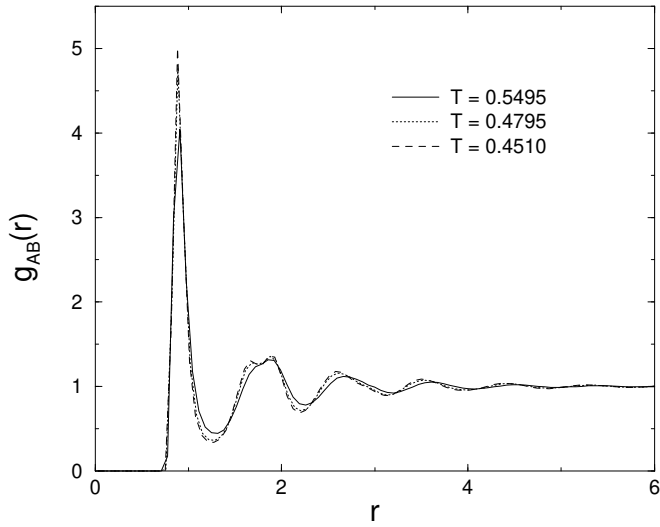


FIG. 3. Pair correlation function $g_{AB}(r)$ between A and B particles for three different temperatures.

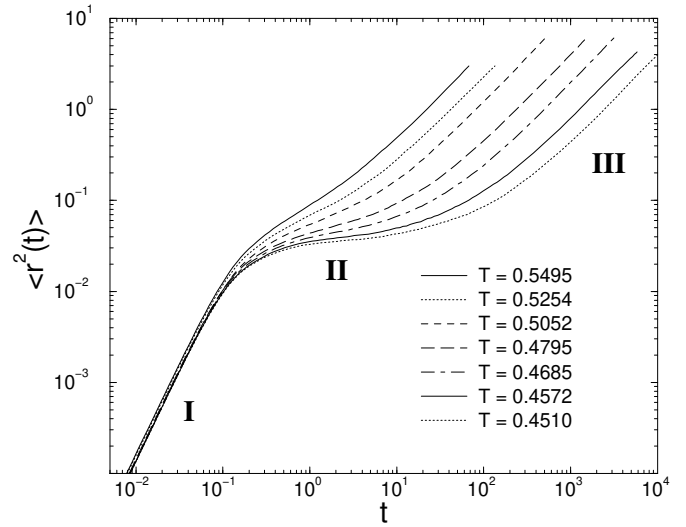


FIG. 5. Mean square displacement $\langle r^2(t) \rangle$ of the A particles vs. time.

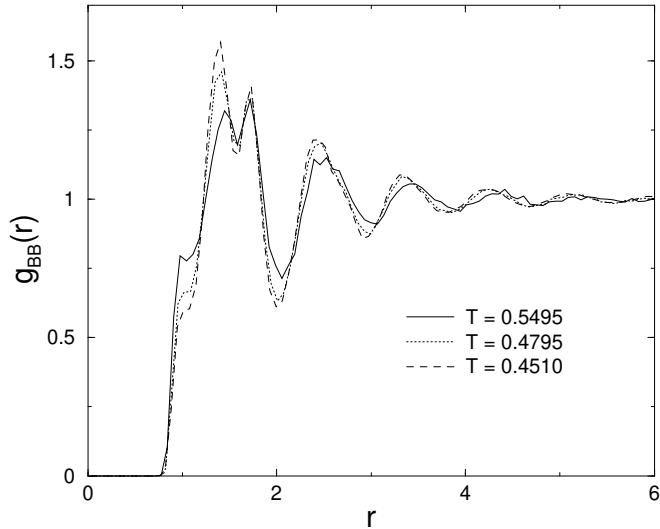


FIG. 4. Pair correlation function $g_{BB}(r)$ of the B particles for three different temperatures.

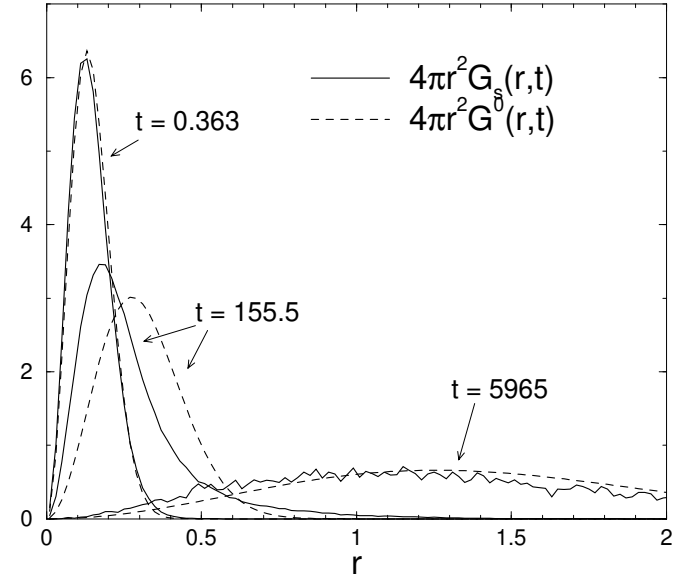


FIG. 6. Solid line: $4\pi r^2 G_s(r, t)$ of the A particles for three times at $T = 0.4510$. Dashed line: Gaussian approximation calculated using the measured $\langle r^2(t) \rangle$ for the same three times.

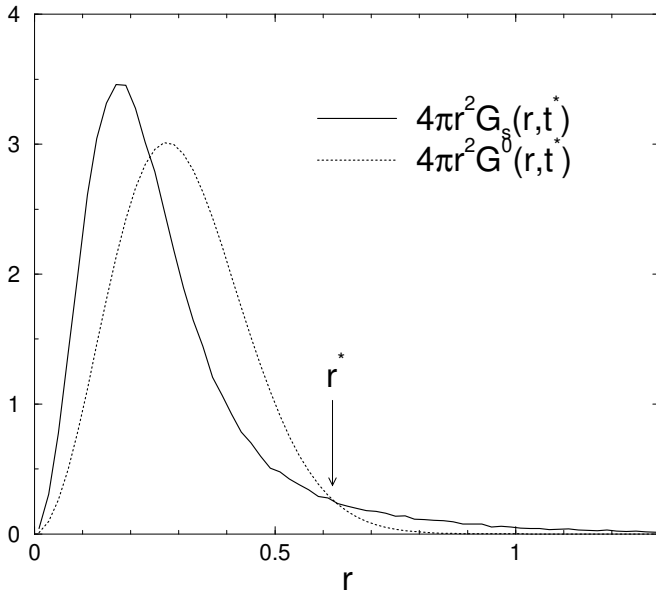


FIG. 7. Same intermediate time data as in previous figure, but enlarged. Solid line: $4\pi r^2 G_s(r, t)$ of the A particles at $t = 155.5$ at $T = 0.4510$. Dashed line: Gaussian approximation calculated using the measured $\langle r^2(t) \rangle$ for the same time.

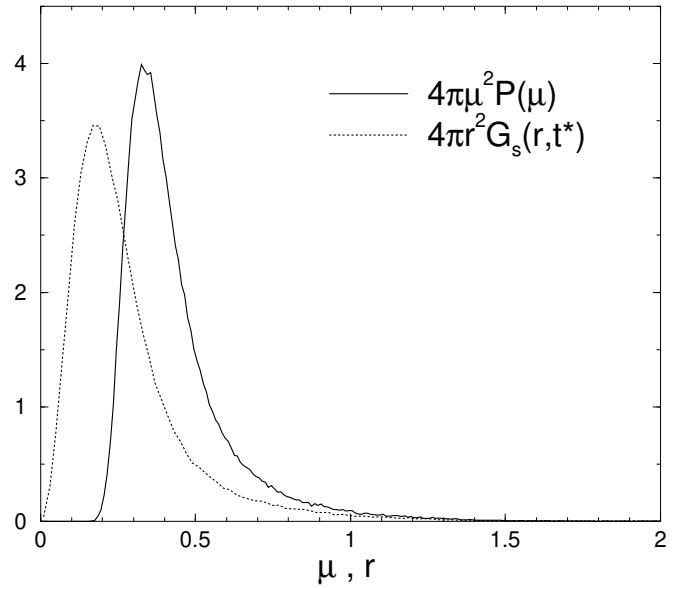


FIG. 9. Probability distribution $4\pi\mu^2 P(\mu, t^*)$ (dashed line) of a particle having a maximum displacement of magnitude μ at t^* . For comparison, the distribution $4\pi r^2 G_s(r, t^*)$ is also shown.

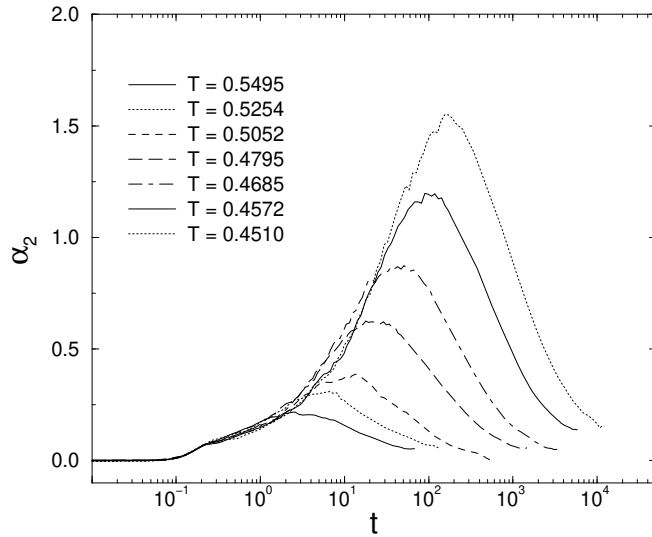


FIG. 8. Non-Gaussian parameter $\alpha_2(t)$ vs. time for different temperatures.

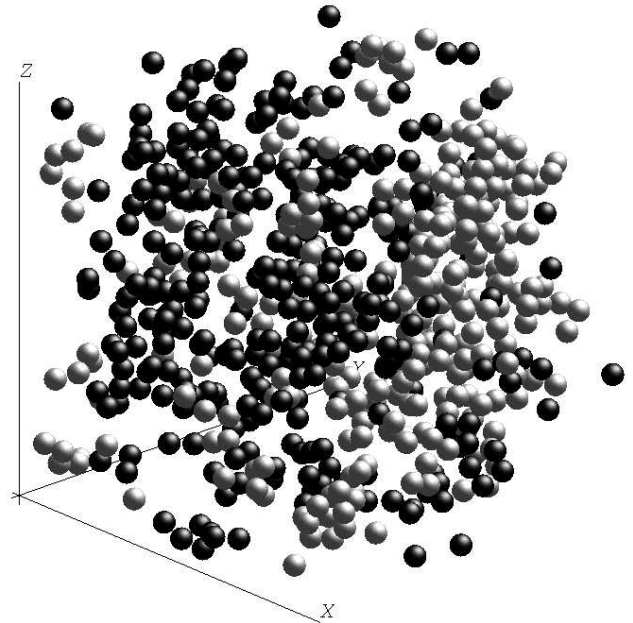


FIG. 10. The 320 mobile particles (light spheres) and the 320 immobile particles (dark spheres) in a configuration at an arbitrarily chosen time.

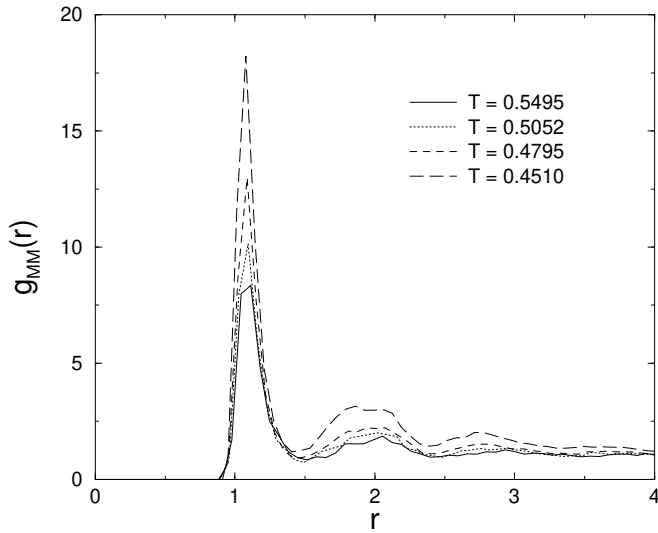


FIG. 11. Pair correlation function $g_{MM}(r)$ between mobile A particles at four different temperatures.

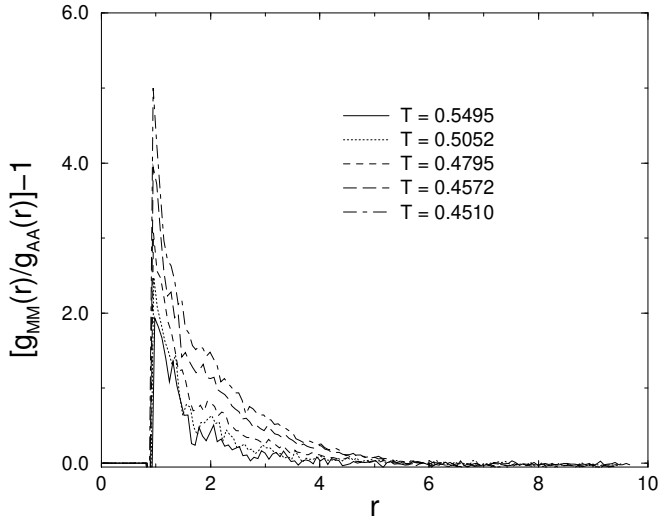


FIG. 12. $\Gamma(r) = [g_{MM}(r)/g_{AA}(r)] - 1$ vs. r for different temperatures.

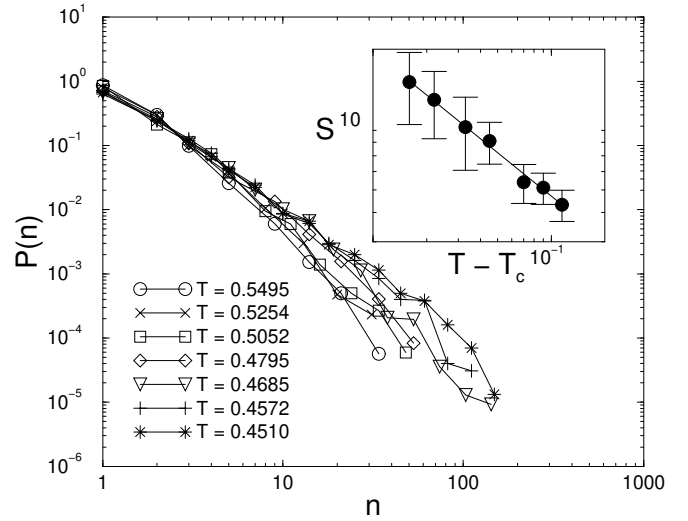


FIG. 13. Distribution of the size n of clusters of mobile particles. Inset: Mean cluster size S plotted versus $T - T_c$, where is the fitted MCT critical temperature $T_c = 0.435$. The straight line is a power law fit $S \sim (T - T_c)^{-\gamma}$, with $\gamma = 0.618$.

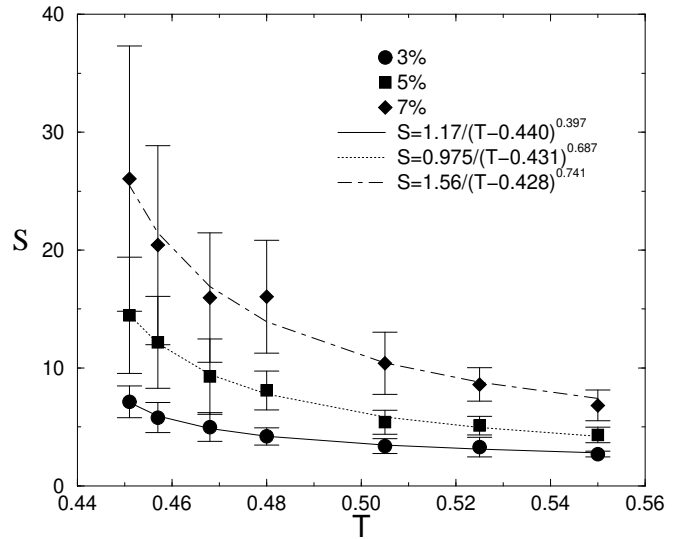


FIG. 14. Mean cluster size S plotted versus T , for subsets containing 3%, 5% and 7% of the most mobile particles. The data for the 5% are the same as those shown in the inset of the previous figure. The lines are power law fits $S \sim (T - T_p)^{-\gamma}$. Best fit parameters are $T_p = 0.440, 0.431$ and 0.428 , respectively, and $\gamma = 0.397, 0.687$, and 0.741 , respectively.



FIG. 15. One of the largest clusters of mobile A particles found at $T=0.4510$. The cluster is composed of 125 particles, which are represented here as spheres of radius $r = 0.5\sigma_{aa}$.

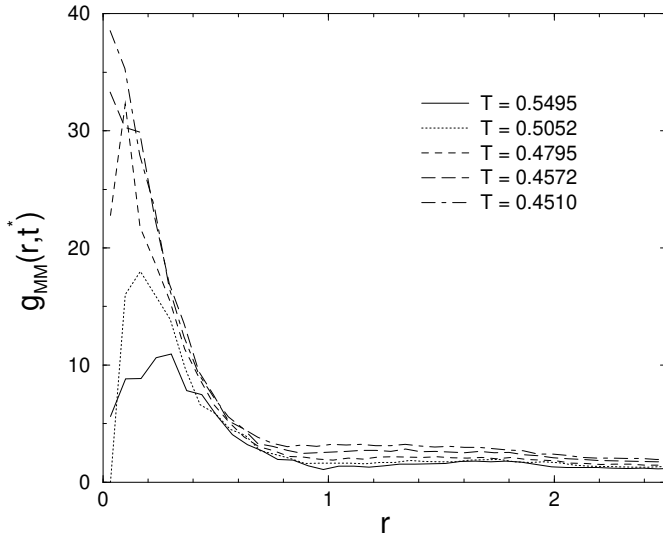


FIG. 16. Time-dependent pair correlation function $g_{MM}(r, t^*)$ vs. r , for different temperatures.

FIG. 17. A cluster of mobile particles at $t = 0$ (light spheres) and $t = t^*$ (dark spheres), for $T = 0.4510$.

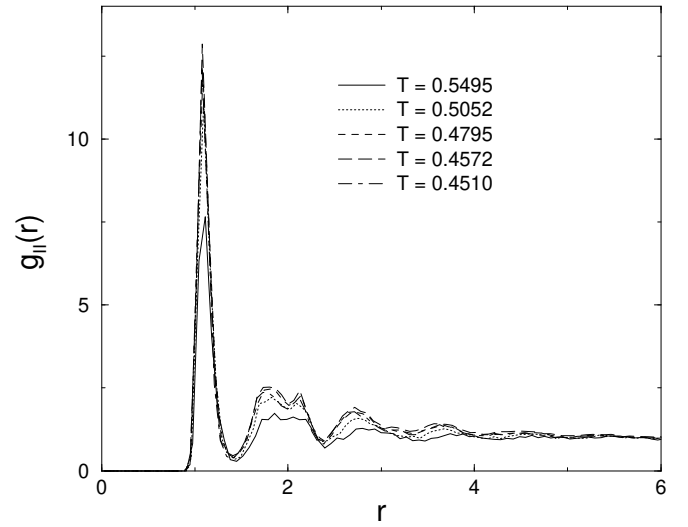


FIG. 18. Pair correlation function $g_{II}(r)$ between immobile particles.

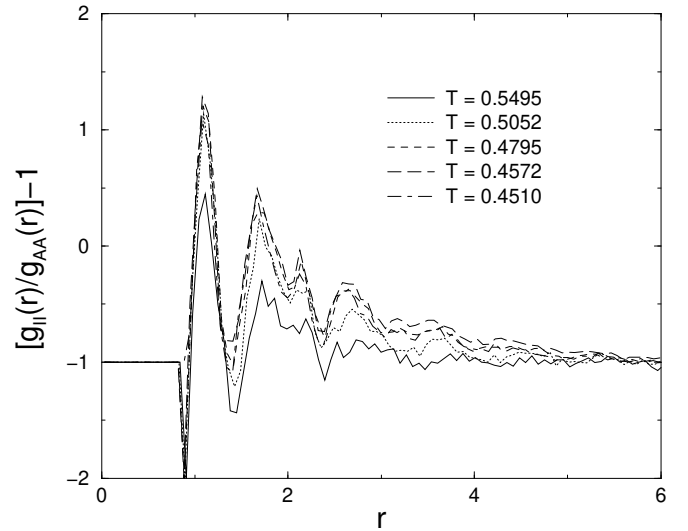


FIG. 19. $\Gamma(r) = [g_{II}(r)/g_{AA}(r)] - 1$ vs. r for different temperatures.

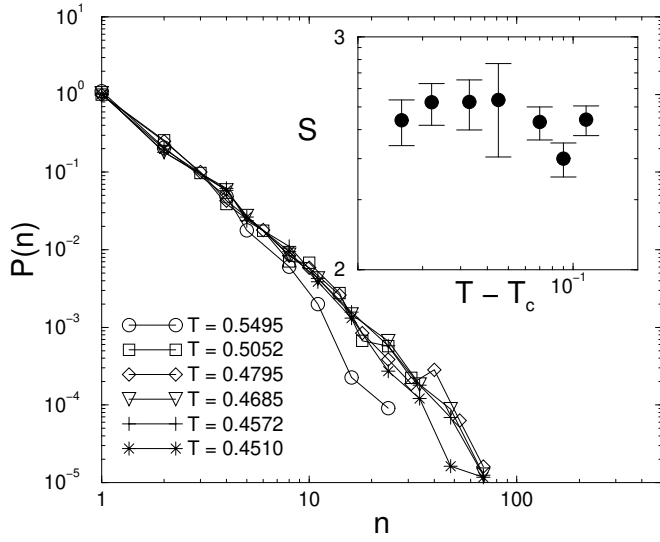


FIG. 20. Distribution of the size n of clusters of immobile particles. Inset: mean cluster size S plotted vs. $T - T_c$.

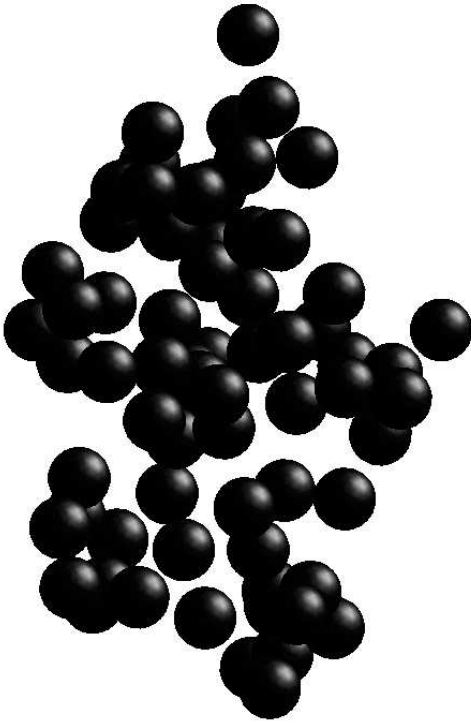


FIG. 21. One of the largest clusters of immobile A particles found at $T=0.4510$. The cluster is composed of 70 particles, which are represented here as spheres of radius $r = 0.5\sigma_{aa}$.

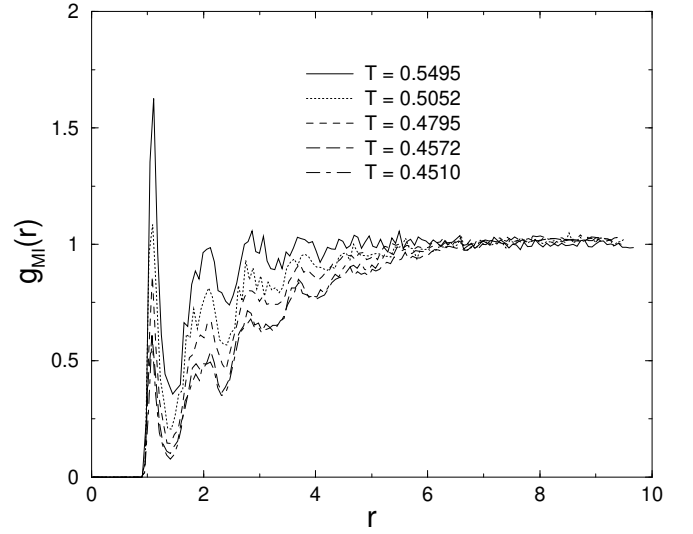


FIG. 22. Pair correlation function $g_{MI}(r)$ between mobile and immobile A particles.

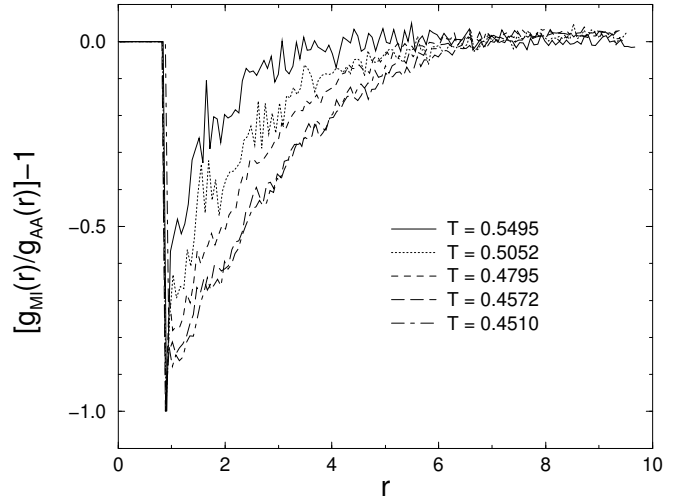


FIG. 23. $\Gamma(r) = [g_{MI}(r)/g_{AA}(r)] - 1$ vs. r for different temperatures.

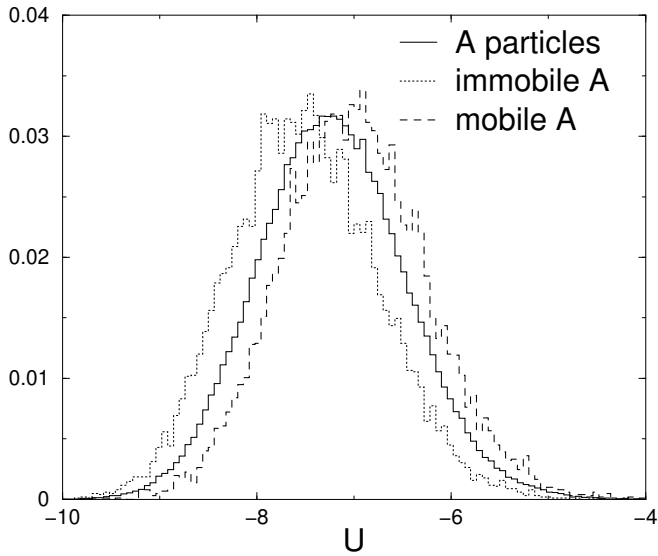


FIG. 24. Distribution of the potential energy of all the A particles, of the mobile A particles and of the immobile A particles for $T = 0.4510$.

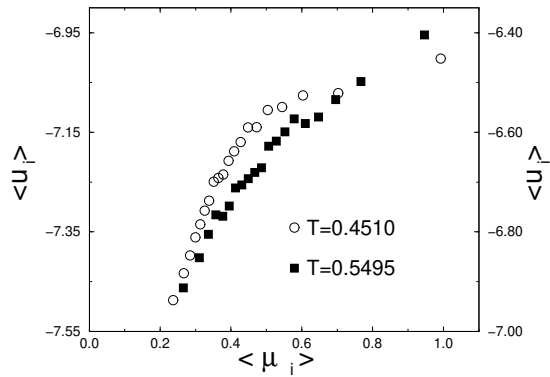


FIG. 25. Potential energy $\langle U_i \rangle$ as a function of the mobility $\langle \mu_i \rangle$ for the A particles. The A particles have been divided into 20 subsets according to their mobility at t^* . Each subset is represented by a point in the graph. The energy scale for $T = 0.4510$ is on the left hand side y axis, while the energy scale for $T = 0.550$ is on the right hand side y axis.

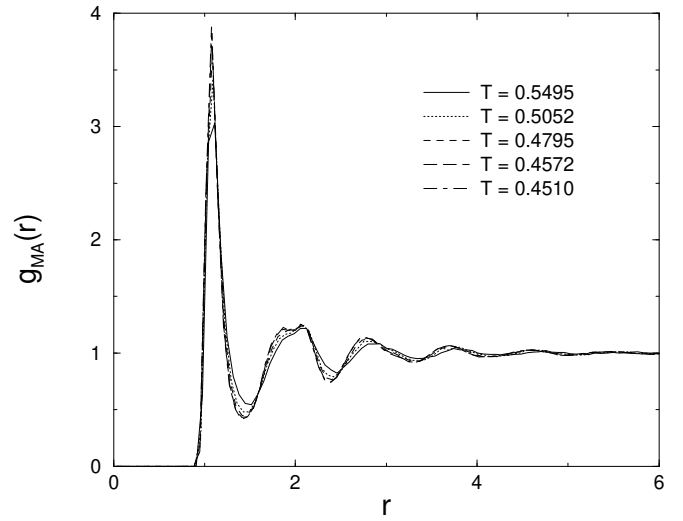


FIG. 26. Pair correlation function $g_{MA}(r)$ between mobile A and generic A particles.

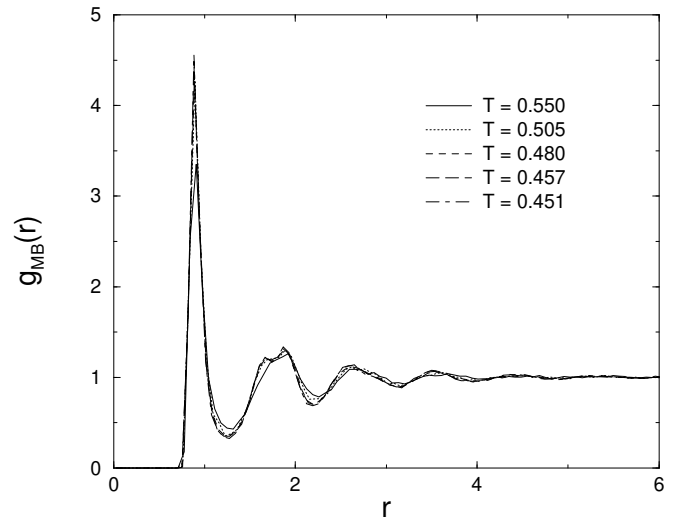


FIG. 27. Pair correlation function $g_{MB}(r)$ between mobile A and generic B particles.

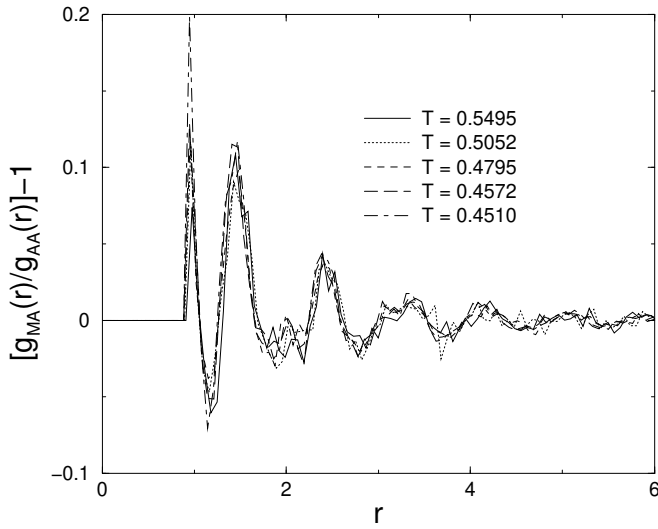


FIG. 28. $\Gamma(r) = [g_{MA}/g_{AA}(r)] - 1$ vs. r for different temperatures.

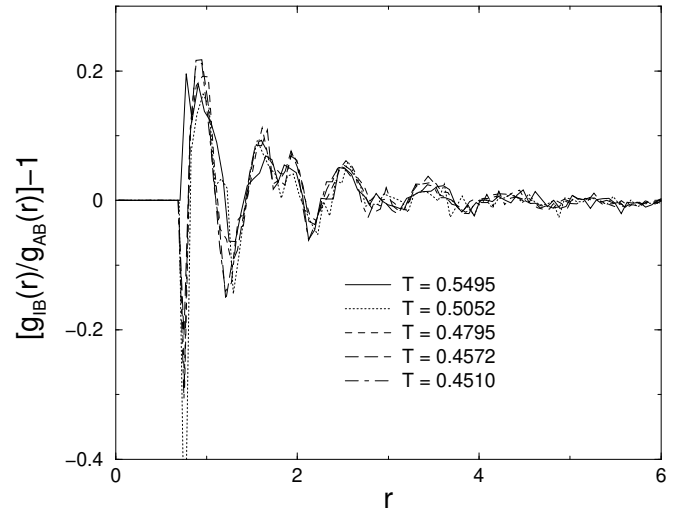


FIG. 30. $\Gamma(r) = [g_{IB}/g_{AB}(r)] - 1$ vs. r for different temperatures.

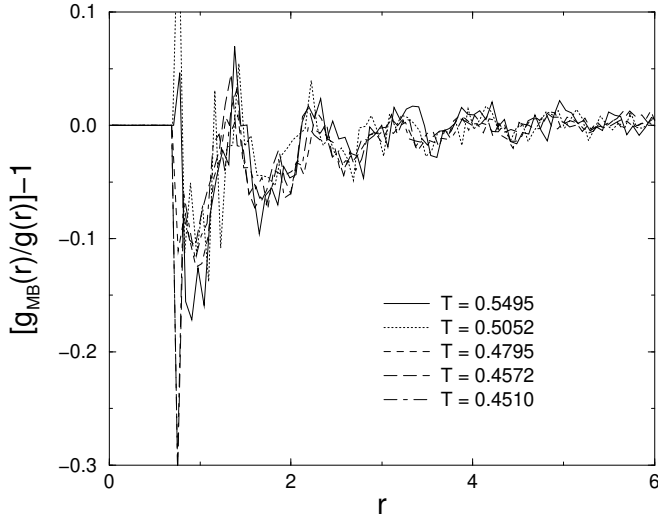


FIG. 29. $\Gamma(r) = [g_{MB}/g_{AB}(r)] - 1$ vs. r for different temperatures.

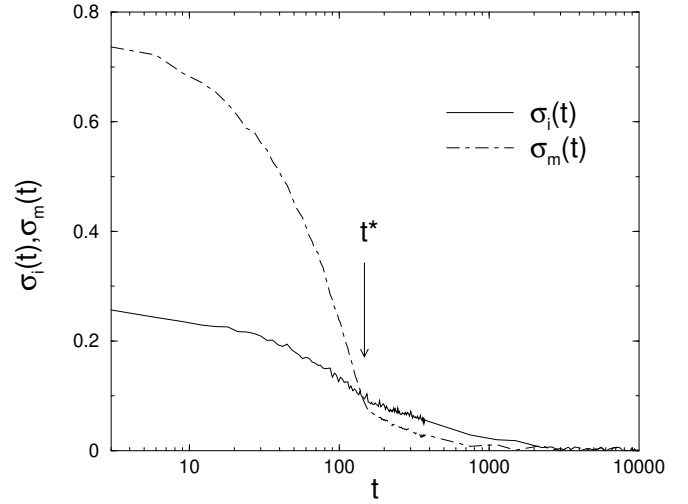


FIG. 31. $\sigma_M(t)$ (dot-dashed line) and $\sigma_I(t)$ (solid line) for $T=0.4510$.

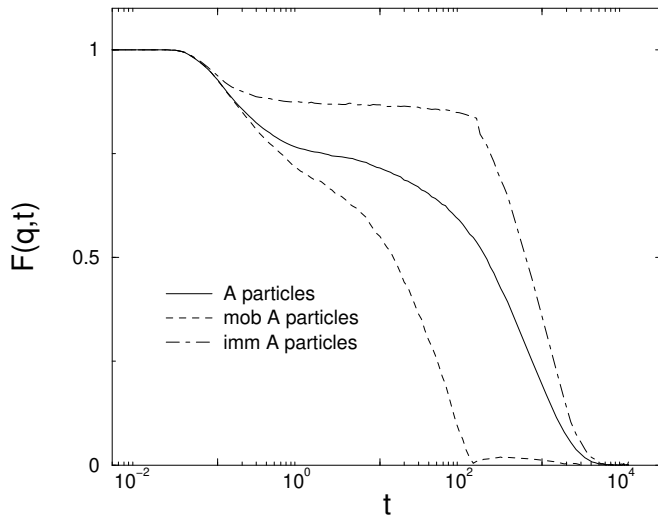


FIG. 32. Self intermediate scattering function for $T=0.4510$ for all the A particles (solid line), for the mobile particles (dashed line) and for the immobile particles (dot-dashed line).

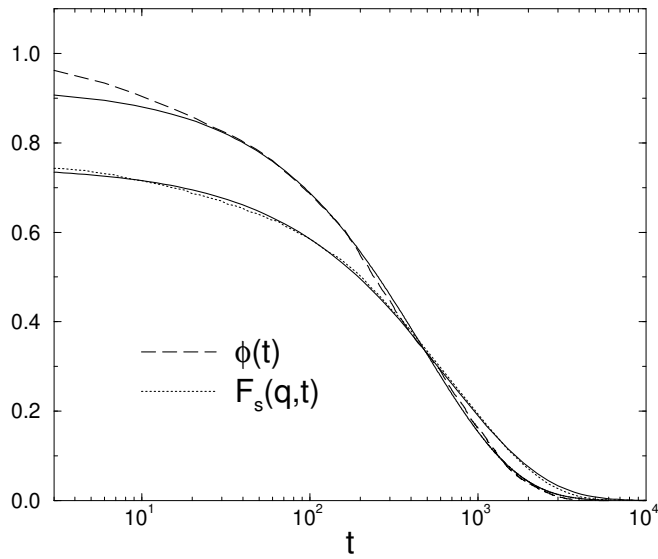


FIG. 33. $\phi(t)$ (dashed line) and $F_s(q,t)$ (dotted line) for $T=0.4510$. The solid lines are fits to a stretched exponential.